Water diffusion in zeolite 4 *A* beds measured by broad-line magnetic resonance imaging

P. D. M. Hughes and P. J. McDonald*
Department of Physics, University of Surrey, Guildford, Surrey GU2 5XH, United Kingdom

M. R. Halse and B. Leone
Physics Laboratory, University of Kent at Canterbury, Canterbury, Kent CT2 7NR, United Kingdom

E. G. Smith
Unilever Research Laboratories Port Sunlight, Quarry Road East, Bebbington, Wirral L63 3JW, United Kingdom
(Received 24 October 1994)

Broad-line magnetic resonance imaging has been used to monitor water transport in beds of industrial grade zeolite 4 *A*. Diffusion profiles as a function of time have been obtained for a series of temperatures in the range 20–70 °C. The dynamics is observed to be strongly non-Fickian. A model based on coupled diffusion equations for the vapor in the interparticle space and water within the particles has been developed and shown to be in good agreement with experiment. Values for the intraparticle water diffusion coefficient and the interparticle vapor diffusion coefficient, which can be obtained from the model, and their respective temperature dependencies are in good agreement with other published results.

INTRODUCTION

An understanding of the diffusion of liquids in porous media is of considerable technological importance. There is already a very substantial body of literature covering systems as diverse as biological materials, oil and water in rocks, cements, concretes, polymers, and zeolites. In zeolites the diffusion occurs over a very large range of length scales[1,2] which can be broadly categorized as intracage or nanometer, intracrystalline or micrometer, and intercrystalline or millimeter. The diffusion can be measured either directly or indirectly on all these scales using a variety of magnetic resonance techniques. Relaxation time studies primarily probe the intracage motion, while the addition of a pulsed field gradient permits measurement of intracrystalline motion. Much early effort was expended on interpreting microscopic self-diffusion magnetic resonance results and rationalizing them with the results of larger scale transport diffusion experiments such as mass absorption.[3] It is now widely appreciated that in complex porous systems, such as zeolites, in which there is an interaction between the diffusing species and the absorbent, anomalous diffusion is observed. In these systems, transport and self-diffusion are different and generally only coincide under special conditions of low diffusant concentration.[4] In this work we concentrate on studying water transport diffusion over macroscopic distances in industrial grade zeolite 4 *A* using magnetic resonance imaging. This is a recent area of study and builds on work of Karger, Seiffert, and Stallmach[5] and our own preliminary studies.[6] Karger, Seiffert, and Stallmach used profiling techniques to show that hexane vapor diffuses according to Fickian dynamics into a previously evacuated zeolite bed. The hexane absorption isotherm is approximately rectangular for the zeolite studied, so that just behind the point of furthest vapor advance the hexane concentration in the zeolite is uniform while ahead of it the concentration is zero. Accordingly, there is a sharp, rectangular, liquid diffusion front in the zeolite bed. The assumption of a rectangular isotherm implies that the hexane flux diffusing through the saturated bed must be independent of distance from the front. Karger, Seiffert, and Stallmach show that this assumption leads very generally to a diffusion front which advances with time as $t^{1/2}$. The rate of front advance agrees well with a theory involving a number of known constants describing their system. Within the imaging experiment Karger, Seiffert, and Stallmach included localized orthogonal pulsed field gradient self-diffusion measurements. These showed that the hexane self-diffusion coefficient within the particles is dependent only on hexane concentration and is independent, in particular, of history.

In contrast, Bansal and Dybowski[7] have used ^{129}Xe high-resolution NMR spectroscopy to follow the long-range diffusion of water in a bilayered sample of Ni Na Y zeolite in which one layer is dehydrated and the other hydrated. They inferred evolving Fickian dynamics as a function of time. Karger[8] has suggested, however, that the presence of the probe xenon atoms may significantly affect the results.

The current study differs in a number of important ways from the previous studies. Water rather than hexane diffusing into a bed of zeolite is expected to be different because of the influence of surface interactions between the polar water molecules and the zeolite which will not be present in the case of the nonpolar organic solvent. As a result, the intraparticle coefficient of diffusion of water is depressed at low water concentrations compared to the organic solvent.[9] For the most part, the current study uses a sealed bed with a known nonequilibrium initial water content distribution rather

than a previously evacuated bed opened up to a reservoir. Moreover, in the current study, the gas between the particles is not pure vapor but low concentration water vapor in air. We have previously noted that equilibration of such a system can be surprisingly slow. For instance, at 10 °C no noticeable transport was observed in a bed approximately 1 cm deep over three days.[6] In this study measurements have been made as a function of temperature. As the temperature is raised the diffusion rate increases. The results show a liquid diffusion front which is neither rectangular, as observed by Karger, Seiffert, and Stallmach, nor Fickian. A model, significantly different from that of Karger, Seiffert, and Stallmach, has therefore been developed to explain the results.

A major and very common problem with imaging fluids confined in porous media is the broad NMR resonance linewidth. The broad line results either directly from the confinement of the nuclei within pores or indirectly from a T_2^* effect due to localized magnetic-field inhomogeneities induced by differences between the magnetic susceptibilities of the material of the pore walls and liquid. The problem can be made worse by paramagnetic impurities.[10] For hydrated industrial grade zeolite 4A the proton resonance has two spin-spin relaxation time (T_2) components—one with a T_2 of about 150–200 μs and the other with a T_2 of about 1.5–2 ms. The components are in the intensity ratio of approximately 1 to 3, respectively, measured at 20 MHz and full hydration. The relaxation behavior varies with hydration level, temperature, and zeolite batch. In general, at low hydrations the short component dominates. The batch dependence results from variations in paramagnetic impurity concentrations. Quantitative imaging of diffusion processes requires that all the hydrogen protons in the system are visualized. Unlike hexane in NaX zeolite, both the proton T_2 components in hydrated zeolite 4A are relatively short and prohibit the use of conventional liquid state magnetic resonance imaging for quantitative studies. A short T_2 imaging protocol is therefore required. This has been achieved in the current study by the use of a variant of the broad-line gradient echo method[11] with an echo time of just 216 μs. To our knowledge, this is the first time that such a technique has been applied quantitatively to the study of diffusion in zeolites.

EXPERIMENT

Industrial grade powdered zeolite 4A with a mean particle size of 3 μm was used throughout this study. Water was removed from a bed of the zeolite, approximately 6 mm deep and loosely packed in a flat bottomed NMR tube, by drying for a period of 48 h at 200 °C. The remnant hydration was typically less than 2% as determined by gravimetric means. Zeolite hydrated in the laboratory atmosphere to 22% was then packed on top of dehydrated material so as to make a total bed typically 12 mm deep with a hydration step halfway down. The free volume in the sample tube was filled by a glass rod and the sample sealed with epoxy resin. The internal diameter of the tube was 20 mm. The samples were profiled periodically at the magnet bore temperature of 10 °C and stored between these measurements at elevated temperature in a temperature controlled oven. Subsequent references to temperature refer to the storage temperature. In order to minimize the time out of the oven, the samples were quenched in cold water immediately prior to profiling. Typically they were out of the oven for 20 min for each measurement. Since previous studies have shown no apparent diffusion over a period of days at 10 °C this procedure is not expected to have significantly affected the results. A repetitive pulse variant of broad-line gradient echo imaging was used to profile the samples.[12] The method is particularly suited to bound fluid systems with T_2 values in the range 100–1000 μs. The pulse sequence is described fully in Ref. 12 and is therefore only briefly summarized here. Figure 1 shows the radio frequency pulse and gradient timing diagram. Sub-90° pulses are applied every m ($m>2$) cycles of a sinusoidally oscillating gradient at a gradient zero crossing and a gradient echo recorded one cycle later. Echoes from each of n continuously applied repeats are summed and averaged. The echo is linearized and Fourier transformed to yield the profile. The total number of repetitions, n, and the repeat interval $m\tau$ are optimized for maximum signal to noise given the constraints of the spin-lattice relaxation time (T_1) and of gradient duty cycle. Since the pulses are sub-90° it is possible to have $m\tau \ll T_1$ allowing rapid averaging.[13] The signal to noise is typically one to two times that available by single shot methods with full 90° pulses for the same total imaging time. More importantly, however, since the pulses are short, they have a high bandwidth which dramatically reduces systematic errors resulting from gradient-induced imperfect rotations. The profiles discussed in this work were all recorded with $m=5$, $n=2000$, $\tau=216$ μs, $g_{max}=30$ G/cm, and with a Larmor frequency of 30 MHz.

Figure 2 shows a representative selection of profiles recorded as a function of time at 22 °C. Profiles are shown for 0, 12, 24, and 36 h. The hydrated layer of the bed on the right, between 0.5 and 1.2 cm, is clearly visible in the first profile of the series recorded at time zero. Subsequent profiles show the diffusion of water from right to left and the later profiles show clearly the other

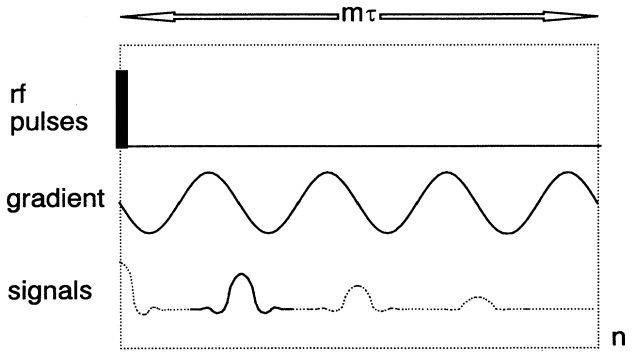

FIG. 1. The magnetic resonance repetitive pulse gradient echo sequence used to record the water in zeolite diffusion profiles.

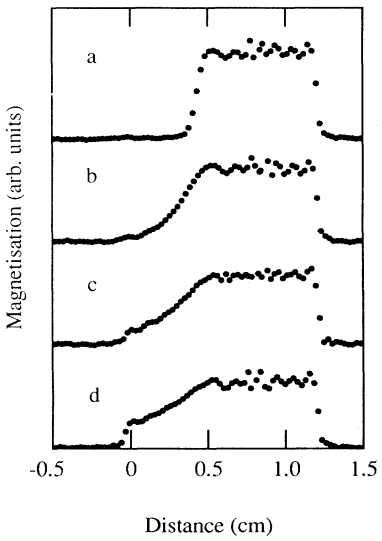

FIG. 2. Experimental water in zeolite diffusion profiles recorded from a zeolite 4A bed after (a) 0 h, (b) 12 h, (c) 24 h, and (d) 36 h at 22 °C. Initially only the hydrated bed between 0.5 and 1.2 cm is seen. As water diffuses into the dehydrated bed, this too becomes visible in the profiles between 0 and 0.5 cm.

end of the sample on the left at $x=0$ cm. The last profile shows the almost equilibrated system. The integrated areas of all the profiles in any one constant temperature series vary by no more than $+/-5\%$, and tend to decrease with diffusion time. With an imaging echo time of 216 μs, a small loss of integrated signal is expected on the basis of an increase in the absolute amount of the short T_2 component. Fully hydrated zeolite has two T_2 components typically of 2000 and 150 μs in the intensity ratio 0.75 to 0.25 while the 50% hydrated material has two components of 1500 and 250 μs of equal intensity. In evolving from fully hydrated zeolite occupying half the volume of the sample to 50% hydrated zeolite occupying all the volume of the sample, the loss in integrated signal due to an increase in the short T_2 component is expected to be of order 10%, in agreement with experiment.

ANALYSIS

Water transport through the bed occurs by vapor diffusion in the intracrystalline space and by liquid phase transport within the particles. There is continual exchange of water between the vapor and the particles. Two coupled partial differential diffusion equations can be written for the water vapor in the intercrystalline space and for the water in the particles. The equations are

$$\frac{\partial C_v}{\partial t}=\frac{\partial}{\partial x}\left[D_v\frac{\partial C_v}{\partial x}\right]-\frac{\partial S}{\partial t}\,,$$

$$\frac{\partial C_p}{\partial t}=\frac{\partial}{\partial x}\left[D_p\frac{\partial C_p}{\partial x}\right]+\frac{\partial S}{\partial t}\,, \tag{1}$$

where t is time and x is depth within the bed. C_v and C_p are the water concentrations in the vapor and particles, respectively. Both are functions of x and t. D_v and D_p are the corresponding diffusion coefficients and are considered constants. $\partial S/\partial t$ is the rate of transfer of molecules from the vapor to the particles. Equations of this form are not new and have been widely used and developed for other applications.[14,15] However, this is the first time that they have been used in this context. Since the particles are small, the hydration level within them remains in absorption equilibrium with the surrounding vapor pressure, according to the absorption isotherm, on a local scale throughout the bed. The transfer term is unknown but can be eliminated by addition of the two equations.

Given that the absorption isotherm for water in zeolite 4A can be approximated by

$$C_v=C_v^0\exp\left[\frac{C_p}{C_p^0}\right] \tag{2}$$

and noting that

$$\frac{\partial C_v}{\partial x}=\frac{dC_v}{dC_p}\frac{\partial C_p}{\partial x} \tag{3}$$

and that $C_p \gg C_v$, Eqs. (1), (2), and (3) lead to

$$\frac{\partial C_p}{\partial t}=\frac{\partial}{\partial x}\left[D_{\text{eff}}\left[\frac{\partial C_p}{\partial x}\right]\right]\,, \tag{4}$$

where

$$D_{\text{eff}}=\left[\frac{D_vC_v^0}{C_p^0}\exp\left[\frac{C_p}{C_p^0}\right]+D_p\right]\,. \tag{5}$$

Equation (4) thus describes the water concentration in the zeolite particles in terms of an effective diffusion coefficient, D_{eff}, itself dependent on the intraparticle and vapor diffusion coefficients and the absorption isotherm. The constants $C_v^0=4.03\times10^{10}$ cm^{-3} and $C_p^0=8.59\times10^{20}$ cm^{-3} have been derived from the absorption isotherm as given by Breck.[16] Writing $X=x/l$, where l is the sample length, $T=D_pt/l^2$, $k=D_vC_v^0/D_pC_p^0$, and $c=C_p/C_p^0$, allows Eq. (4) to be written in a dimensionless form as follows:

$$\frac{\partial c}{\partial T}=\frac{\partial}{\partial X}\left[[1+k\exp(c)]\frac{\partial c}{\partial X}\right] \tag{6}$$

in which the sample resides between $X=0$ and 1. This dimensionless equation is one of a class of equations considered by Barrer[17] in which $D_{\text{eff}}=D_0[1+f(c)]$. The case that $f(c)=a\exp(bc)$, $a,b=$const, was specifically considered by Barrer but not for the boundary conditions appropriate to our study. Equation (6) can be numerically integrated to yield a set of absorption profiles as a function of time given appropriate starting and boundary conditions and the constant k.

The following procedure has been adopted for analyzing the profiles. First the value of $c=c_0$ for the fully hydrated zeolite has been estimated and the amplitude of

the first profile in a temperature series scaled accordingly. Based on an estimated relative humidity of 50% in the laboratory, a value of c_0 of 15.8 has been deduced.[18] Best fits to the data, however, have been obtained for a slightly higher value of 16.5. At the same time as normalizing the first profile intensity to c_0, the area under each profile in a given temperature series has been normalized to the area of the first profile recorded at the start of the experiment. This partially corrects for the loss in signal intensity with time resulting from the decrease in average T_2 of the sample. In no case was this a large change. The fractional depth of the dehydrated bed at the start, X_1, has been measured for each sample from the initial profiles. The initial, $T=0$, theoretical profile has been set as $c=0$, $0 \le X < X_1$; $c=c_0$, $X_1 \le X \le 1$. The dimensionless diffusion equation has been solved numerically for various values of k in the range $10^{-3} > k > 10^{-7}$ to yield $c_k(X,T)$, with the subscript k indicating the value used. Care was taken to ensure that the time and space steps used in the numerical integration were small enough to ensure convergence of the results.

For each temperature series, the experimental profile where the intensity at the dry end of the bed, $X=0$, had risen to approximately 25% of c_0 (i.e., c approximately 4) was selected. This profile corresponds to one for which the bed equilibration is approximately half complete. Earlier and later profiles are less sensitive to the fitting parameters. The theoretical profile $c_k(X,T)$, which simultaneously matched the data at both ends, $X=0$ and $X=1$, of the chosen profile was judged to give the best fit. As two values of c are being fitted, and there are two variable parameters, k and T, the solution to this is unique for a given value of c_0. However, given the numerical method of solving the equation, the finite number of k and T values inspected and noise in the chosen profile, a degree of judgment is required in selecting the best-fit parameters. The k value was subsequently kept constant for that temperature series. Theoretical profiles for T values scaled according to the experimental times, t, of the other profiles in the series were identified and compared to the data. Poor fits to these profiles indicated that the value of c_0 needed adjustment.

Figures 3, 4, and 5 show two representative experimental profiles and theoretical fits for zeolite beds at temperatures of 33, 52, and 70 °C. The fit parameters for all the samples are summarized in Table I. From the fit parameters, the actual profiling times, and the sample lengths it is possible to calculate D_p and D_v using the definitions of k and T. These are also included in Table I. The intraparticle diffusion coefficient varies systematically with temperature over almost two orders of magnitude yet for any one temperature series both of the calculated

TABLE I. Parameters used in fitting the experimental profiles. The bottom two rows are for the open-ended sample experiments [Figs. 6(a) and 6(b)].

Temp. (°C)	l (cm)	X_1	k (10^{-5})	D_p (10^{-5} cm^2 s^{-1})	D_v (cm^2 s^{-1})
22	1.2	0.35	5.6	0.022	0.26
33	1.25	0.40	2.4	0.027	0.14
40	1.2	0.35	1.8	0.051	0.19
47	1.3	0.35	0.56	0.11	0.13
52	1.25	0.35	0.32	0.26	0.18
57	1.25	0.35	0.32	0.48	0.33
70	1.25	0.50	0.056	1.98	0.24
20	2.00	open-ended	2.5	0.042	0.22
20	10.00	open-ended	2.5	0.060	0.32

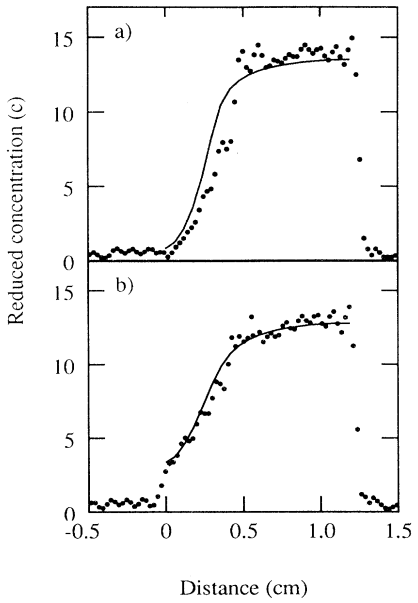

FIG. 3. Two experimental profiles recorded at 33 °C and after (a) 8 h and (b) 24 h together with theoretical fits according to the model described in the text.

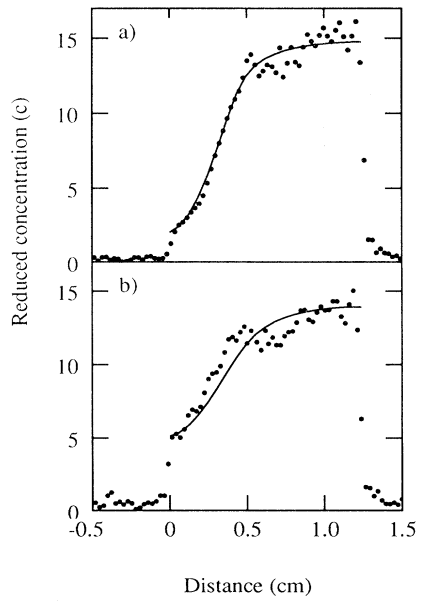

FIG. 4. Two experimental profiles recorded at 52 °C and after (a) 1.83 h and (b) 3.66 h together with theoretical fits according to the model described in the text.

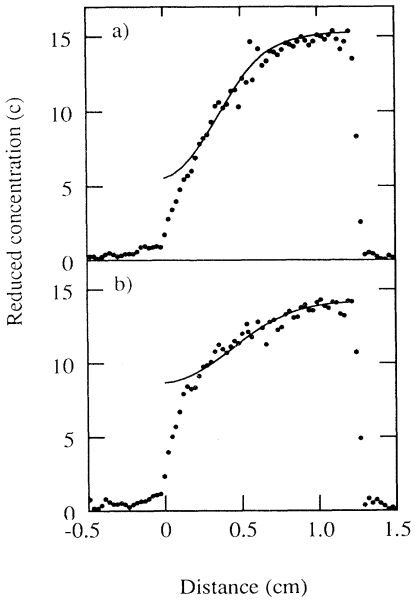

FIG. 5. Two experimental profiles recorded at 70 °C and after (a) 1.58 h and (b) 3.41 h together with theoretical fits according to the model described in the text.

diffusion coefficients are surprisingly robust to small changes in the constants c_0 and k. Moreover, the quality of the fits is reassuringly high especially given the tight constraints placed on varying parameters within the fitting procedure.

DISCUSSION

The theoretical fits support the claim that the diffusion is non-Fickian. For a typical k value of 10^{-5}, the concentration parameter c must fall to 11.5 (about two-thirds of the fully hydrated value, c_0) before the exponential term in the diffusion coefficient equals the unity term. Only for significantly smaller concentrations that 11.5 can the diffusion be considered Fickian. The diffusion process can be qualitatively interpreted as follows. On encountering a region of partially hydrated zeolite, vapor is absorbed by the particles relatively quickly. If the vapor concentration is high, a square hydration front forms and advances in the zeolite bed at a rate controlled by the vapor supply in an analogous manner to hexane into zeolite as observed by Karger.[5] This process also continues at lower vapor pressures. However, in this case, the rate of front formation is slowed due to the lack of vapor molecules. Low concentration intraparticle diffusion then becomes the dominant process for bulk transport within the bed and the liquid diffusion front acquires a more conventional Fickian profile. This regime was not observed by Karger.

These concepts can be further tested experimentally by observing atmospheric vapor diffusion into a totally dehydrated zeolite bed open at one end, thereby maintaining a high vapor pressure at that end. We have used gradient echo and planar sensitive techniques to profile beds 20 and 100 mm deep at 20 °C. Figures 6(a) and 6(b) shows experimental profiles and theoretical fits recorded from the two samples. For short times, Fig. 6(a), a sharp diffusion front proceeds into the bed linearly with time. Behind the front there is only a small water concentration gradient. At longer times, Fig. 6(b), and as a significant depth of hydrated bed develops, the advance of the diffusion front slows to $t^{1/2}$. For these experiments, the relative humidity at the open end ($x=0$ cm) was measured and the corresponding value of c_0 [14.9 and 16.2 for Figs. 6(a) and 6(b), respectively] was used in the data analysis. The calculated values $D_p=4.2\times10^{-7}$ and $D_v=0.22$ cm^2 s^{-1} from Fig. 6(a) and $D_p=6.0\times10^{-7}$ and $D_v=0.32$ cm^2 s^{-1} from Fig. 6(b) are in good agreement with those deduced from the fitting of the sealed sample profiles; see Table I. The value of k was kept constant at 2.5×10^{-5} since the quality of the long diffusion time data was insufficient to permit detailed fitting of the shape of the diffusion front.

Figure 7 shows that the value of the intracrystalline diffusion coefficient D_p deduced from experiment depends exponentially on temperature, rising from 2.5×10^{-7} cm^2 s^{-1} at 22 °C to 2×10^{-5} cm^2 s^{-1} at 70 °C. By fitting D_p to the expression

$$D_p = D_p^0 \exp\left[\frac{-\theta_0}{\theta}\right], \tag{7}$$

where D_p^0 and θ_0 are constants and θ is the absolute temperature. The activation energy for intraparticle

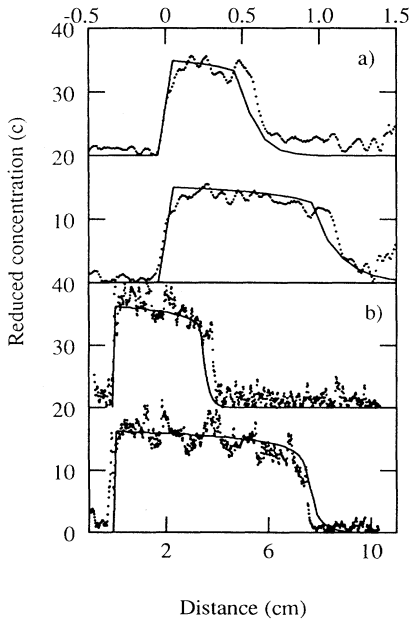

FIG. 6. Water concentration profiles recorded from zeolite beds (a) 20 mm deep after 25 (top) and 50 (bottom) h and (b) 100 mm deep after 191 (top) and 622 (bottom) h, together with theoretical fits. In each case the initially dehydrated bed is open to the atmosphere from the left. The upper traces in both (a) and (b) have been offset by 20. Note the change in horizontal scale between (a) and (b).

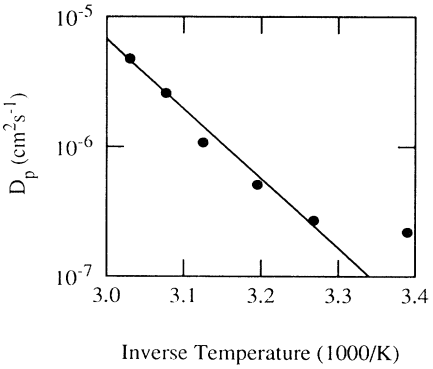

FIG. 7. The temperature dependence of the intraparticle diffusion coefficient D_p for water in zeolite 4A as determined from the theoretical fits to the NMR profiles. The solid line is the best fit to the data used to evaluate the activation energy.

diffusion has been calculated to be $103+/-8$ kJ mol^{-1}. The activation energy and the absolute values of D_p are in good agreement with typical values for similar systems found in the literature. For instance, Pfeiffer *et al.*[19] report D_p values of order 10^{-6} cm^2 s^{-1} for water in zeolite Na*X* at 20 °C while Karger, Zikanova, and Kocirik[20] deduce an activation energy of 58 kJ mol^{-1} for the diffusion of cyclohexane in zeolite Na*X*.

In the model developed in this work it has been assumed that D_p is constant for a given temperature and specifically that it is independent of concentration. This is undoubtedly an oversimplification. Karger[9] has shown that for water at very low coverage in zeolite Na*X*, the intracrystalline diffusion is depressed by bonding of water molecules to adsorption sites due to their electric dipole moments. These same water molecules are the ones which exhibit the shortest spin-spin relaxation times and which are therefore inaccessible even to broad-line magnetic resonance imaging. At higher coverage D_p increases as the bonding sites are filled. In Na*X* zeolite D_p reaches a maximum at a concentration of about 40% of maximum. Above this the void space decreases restricting the opportunity for diffusion and the diffusion constant decreases once more. Except at the very lowest concentrations, variations are by no more than a factor of 2. Undoubtedly improved fits to our data could be obtained by lifting the restriction that D_p be independent of c, but without more details this is little more than an academic exercise at this stage. Moreover, improved fits to the individual profiles could be obtained for any one single profile if the restrictions that c_0 remain constant and T be proportional to t were lifted. The first depends on the humidity in the laboratory, which, although air conditioned, is known to vary over a period of time. The second takes no account of the integrated effects of sample heating and cooling. The experimental time, t, merely reflects the time the sample was in the (preheated) oven.

D_v is of order 0.2 cm^2 s^{-1} and exhibits no significant temperature dependence. Ideal gas kinetics can be used to estimate D_v.[18] The appropriate equation for the diffusion coefficient of water molecules in air is

$$D_v=\frac{3}{8}\left[\frac{\pi}{2}\right]^{1/2}\frac{1}{c_{\text{air}}\pi\sigma^2}\left[\frac{R\theta}{M}\right]^{1/2}, \tag{8}$$

where c_{air} is the total number of air molecules per cc, σ is the effective molecular diameter of an air molecule, R is the gas constant, M is the reduced (center of mass) molecular weight of water molecules in air, and θ is the absolute temperature. Assuming parameters for air to be $c_{\text{air}}=2.49\times10^{24}$ m^{-3}, $\sigma=3.36\times10^{-10}$ m, and $M=18\times28.8/(18+28.8)=11.08$ g, then $D_v=0.25$ cm^2 s^{-1} at 20 °C. An allowance must be made for tortuosity, τ, and zeolite packing density, η, both of which will tend to reduce D_v in the bed. The measured value of D_v is expected to be a factor $(1-\eta)/\tau$ smaller than the free air value. Estimated values for η and τ are 0.33 and 3, respectively, suggesting that the apparent interparticle value for D_v should be of order 4.5 times less than the calculated free air value. However, as can be seen from Table I, the measured values are only a little smaller. It is unclear at this stage whether the discrepancy is due to errors in our estimates for τ and η or in the diffusion model. Note also that, in theory, the $\theta^{1/2}$ factor in Eq. (8) predicts an 8% increase in D_v from 22 to 70 °C. However, this is too small to be resolved in our measurements, especially given the variations in packing density between the samples.

Finally, it is worth reiterating that measurements of water diffusion in these plugs could not have been made using more conventional means such as pulsed field gradient magnetic resonance. This is because the short spin-spin relaxation times found in industrial grade zeolite precludes the generation of PFG spin echoes with sufficiently large pulse gaps. PFG experiments performed with sub-milli-second pulse gaps would not reflect the bulk transport over macroscopic distances but rather would reflect shorter-range self-diffusion within the particles.

ACKNOWLEDGMENTS

P.D.M.H. thanks the United Kingdom Engineering and Physical Sciences Research Council for financial support. B.L. thanks the European Commission for financial support.

*Author to whom correspondence should be addressed.

[1]J. Karger and H. Pfeiffer, Zeolites **7**, 90 (1987).
[2]H. Pfeiffer, Phys. Rep. **26C**, 293 (1976),
[3]J. Karger and J. J. Caro, Chem. Soc. Faraday. Trans. **173**, 136 (1977).
[4]J. Karger, Surf. Sci. **59**, 749 (1976).
[5]J. Karger, G. Seiffert, and F. Stallmach, J. Magn. Reson. **A102**, 327 (1993).
[6]E. G. Smith, J. W. Rockliffe, P. J. McDonald, A. R. Lonergan, M. R. Halse, B. Leone, and J. H. Strange, Magn. Reson. Imag. **12**, 231 (1994).
[7]N. Bansal and C. Dybowski, J. Magn. Reson. **89**, 21 (1990).

[8]J. Karger, J. Magn. Reson. **93**, 184 (1991).
[9]J. Karger, Z. Phys. Chem. **248**, 27 (1971).
[10]H. A. Resing and J. K. Thompson, in *Proceedings of the 15th Congress Ampere, Grenoble, 1968* (North-Holland, Amsterdam, 1969), p. 237.
[11]S. P. Cottrell, M. R. Halse, and J. H. Strange, Meas. Sci. Technol. **1**, 624 (1990).
[12]P. J. McDonald, K. L. Perry, and S. P. Roberts, Meas. Sci. Technol. **4**, 896 (1993).
[13]R. R. Ernst, G. Bodenhausen, and A. Wokaun, *Principles of Nuclear Magnetic Resonance in One and Two Dimensions* (Oxford University Press, Oxford, 1987), p. 124.
[14]J. Crank, *The Mathematics of Diffusion,* 2nd ed. (Oxford University Press, Oxford, 1975), Chap. 14.
[15]M. Sahimi, *Applications of Percolation Theory* (Taylor and Francis, London, 1994), Chap. 8.
[16]D. W. Breck, *Zeolite Molecular Sieves* (Wiley, New York, 1974), p. 607.
[17]R. M. Barrer, Proc. Phys. Soc. **58**, 321 (1946).
[18]E. H. Kennard, *Kinetic Theory of Gases* (McGraw-Hill, New York, 1938), pp. 25, 194, and 203.
[19]H. Pfeiffer, J. Karger, A. Germanus, W. Schirmer, M. Bulow, and J. J. Caro, J. Adsorp. Sci. Technol. **2**, 229 (1985).
[20]J. Karger, A. Zikanova, and M. Kocirik, Z. Phys. Chem. **265**, 587 (1984).